Supplementary Information for

Combustion-Derived Organic Aerosols Enhance $PM_{2.5}$ Oxidative Potential in a Medium-Sized North China Plain City

*Jing Cai[1,2], Yongchun Liu[3], Feixue Zheng[3], Dian Ding[4], Wei Du[5], Liang Yuan[6], Yingjie Zou[7], Lazong Suolang[8], Rongxiang Lu[8], Wanwei Li[8], Chao Liu[1,2], Xiaolong Fan[9,10 *], Qiaozhi Zha[4,11 *], Mengxiao Luan[8 *], Jiandong Wang[1,2]*

1. State Key Laboratory of Climate System Prediction and Risk Management, Nanjing University of Information Science and Technology, Nanjing, 210044, China
2. Collaborative Innovation Center on Forecast and Evaluation of Meteorological Disasters, School of Atmospheric Physics, Nanjing University of Information Science and Technology, Nanjing, 210044, China
3. Aerosol and Haze Laboratory, Beijing Advanced Innovation Center for Soft Matter Science and Engineering, Beijing University of Chemical Technology, Beijing, 100029, China
4. National Observation and Research Station for Atmospheric Processes and Environmental Change in Yangtze River Delta, Nanjing, 210023, China
5. Institute for Atmospheric and Earth System Research, Faculty of Science, University of Helsinki, Helsinki 00014, Finland
6. Chengdu Plain Urban Meteorology and Environment Observation and Research Station of Sichuan Province, School of Atmospheric Sciences, Chengdu University of Information Technology, Chengdu 610225, China
7. Shandong Weifang Provincial Eco-Environmental Monitoring Center, Weifang, 261053, China
8. School of Public Health, Shandong Second Medical University, Weifang 261053, China
9. State Key Laboratory of Advanced Environmental Technology, Institute of Urban Environment, Chinese Academy of Sciences, Xiamen 361021, China
10. Fujian Key Laboratory of Atmospheric Ozone Pollution Prevention, Institute of Urban Environment, Chinese Academy of Sciences, Xiamen 361021, China
11. Nanjing-Helsinki Institute in Atmospheric and Earth System Sciences, Nanjing University, Nanjing, China, 210023

Ramping Protocol for FIGAERO-CIMS

A uniform temperature ramping protocol was applied for all filters, following four steps: (1) stabilization at 25 °C for 1 min; (2) heating from 25 °C to 200 °C in 24 min; (3) soaking at 200 °C for 15 min; and (4) cooling to 25 °C within 15 min. The instrument background was assessed by analyzing data from two heating cycles performed on each filter sample. Meanwhile, parallel experiments were conducted to examine the effects of sampling and operation, with linear regression slopes ranging from 0.84 to 1.13 and the correlation coefficients upwards to 0.997.

Hierarchical Cluster Analysis

Hierarchical Cluster Analysis (HCA) is an unsupervised method that constructs a dendrogram by progressively merging samples to reveal underlying similarity relationships. In this study, HCA was employed to classify OA samples based on their molecular-level composition. The analysis utilized a sample-by-molecule data matrix comprising 48 samples and 274 identified molecular formulas (e.g., $C_{10}H_8O_3$, $C_7H_6O_3$). Prior to clustering, the data were standardized to eliminate magnitude biases and ensure equal weighting of all compounds. The analysis was performed using R software (version 4.4.1). Euclidean distance was used to quantify dissimilarities, combined with Ward's minimum variance method as the linkage criterion. This approach is well-suited for standardized, high-dimensional compositional data and is widely established in aerosol molecular characterization studies [1, 2]. The resulting hierarchical structure was visualized as a dendrogram, with the optimal number of clusters determined based on linkage distance and the chemical interpretability of molecular patterns. These identified clusters represent distinct OA molecular regimes and serve as the basis for subsequent analyses.

Double-bond equivalence calculation

The double-bond equivalence (DBE), oxidation state for the oxygenated organic compounds were calculated as Eq 3 and 4, following Wang et al., 2017 [3, 4].

$$DBE = \frac{2c+2+n-h}{2} \quad \text{Eq. 3}$$

$$OS = 2 \times \frac{o}{c} - \frac{h}{c} \quad \text{Eq. 4}$$

Here, c, n, and h represent the number of carbon, nitrogen, and hydrogen atoms in the compound's chemical formula. with FIGAERO-CIMS.

Positive Matrix Factorization

In this study, positive matrix factorization (PMF) was applied to identify potential sources of ambient $PM_{2.5}$ online $PM_{2.5}$ inorganic component data with OC and EC were imported into the

Source Finder toolkit (SoFi, ver. 6.8.4), which communicates with the multi-linear engine (ME-2). PMF analysis utilized online fine particulate matter component data (average to 1-h resolution, Table S1) collected on the rooftop of the Huanjing Building, situated northeast of the Xinhua Road and Jiankang Road intersection in downtown Weifang. The uncertainty of the PMF input data was calculated using two separate equations, depending on whether the species concentration was above (Eq. 1) or below (Eq. 2) the method detection limit (MDL). In the trace element analyses, the criterion for selection was that data for a given element had to exceed three times the MDL in most samples. Therefore, the PMF analysis was limited to 11 elements: Al, K, Ca, Ti, Mn, Fe, Co, Cu, Zn, Se, and Pb.

A total of seven sources were resolved in this study, including secondary inorganic aerosols, vehicle emissions, coal combustion, biomass burning, fireworks and related emissions, industrial emissions, and dust. Detailed sampling information regarding the source apportionment analyses will be discussed in Luan et al. (in preparation).

$$Uncertainty_{i,j} = \sqrt{(\text{Error Fraction} \times \text{Conc}_{i,j})^2 + (0.5 \times MDL_i)^2} \quad \text{Eq. 1}$$

$$Uncertainty_{i,j} = \frac{5}{6} \times MDL_i \quad \text{Eq. 2}$$

Here, Uncertainty and Conc represent the uncertainty and concentration of species *i* in sample sequence *j*. MDL denotes the method detection limit for species *i*. An error fraction of 20% was applied in this study.

The variation in Q/Qexp values suggested that five factors could explain the majority of the residuals, as adding additional factors did not further decrease the ratio. Introducing more factors only added a component dominated by noise stemming from the variation of trace elements due to instrumental analytical uncertainty. Fpeak tests were conducted within a range of -1 to 1 (increments of 0.1). Compared to the base runs, Fpeak rotation primarily altered the separation and profiles of the factors, particularly for dust sources.

Secondary inorganic sources were identified due to high concentrations of secondary components, such as nitrate, ammonium, and sulfate. Vehicle emission factor was enriched in nitrate but showed lower contributions of SO_4 or K^+, indicating a strong influence of nitrogen emission related sources which differ from biomass burning activities. The co-variation of this factor with gaseous pollutants, such as CO and NO, during the early morning suggested that vehicle emissions were the primary source. In contrast, the source profile of coal combustion exhibited higher levels of crustal elements (e.g., Al, Ca, and Fe) except for carbonaceous aerosols; the presence of these trace metals suggests that this factor originated from coal burning rather than vehicle emissions. This was further validated by the high correlation between coal combustion and sulfur-containing organics (discussed in Main Text 3.3). Additionally, the coal combustion factor peaked later than CO and NO_2 around 11:00 AM, which was close to the SO_2 peak, implying an origin linked to coal combustion. The biomass burning profile was characterized by high levels of OC and EC, along with an abundance of K^+, NO_3^-, and Cl^-, which are key inorganic tracers of biomass burning activities. The strong correlation between organic tracers (e.g., levoglucosan and nitrocatechols) and this factor further confirmed its likely origin from biomass burning activities (discussed in Main Text 3.3). The dust factor was distinguished by a high abundance of crustal elements, such as Ti, Ca, and Al. Its time series peaked only during three extreme episodes on March 17, 19, and 28, with PM_{10} concentrations of 490, 451, and 666 μg m^{-3}, respectively, while

$PM_{2.5}$ concentrations remained less than 100 μg m^{-3}. The low contribution of EC and the correlation between OA and this factor suggest that this source is primarily crustal dust.

Table S1. Online instrumentation used in this study

Species	Time resolution	Instrument information
BC, and TC, therefore, OC is calculated as their difference, and OA is calculated as 1.4 times OC	1-hour	Carbonaceous Aerosol Speciation System (TCA-08, Magee Inc. USA)
Trace Metals (Al, K, Ca, Ti, Mn, Fe, Co, Cu, Zn, Se, Pb)	1-hour	Online trace metal analyzer (AHMA-1000, NCS Testing Technology Co., Ltd. China)
Water-soluble ions (NO_3^-, SO_4^{2-}, NH_4^+, K^+, Mg^{2+}, Ca^{2+}, Na^+, Cl^-)	1-hour	In-situ Gas and Aerosol Composition monitoring system (Model S-611, Fortelice International Co., Ltd. China).

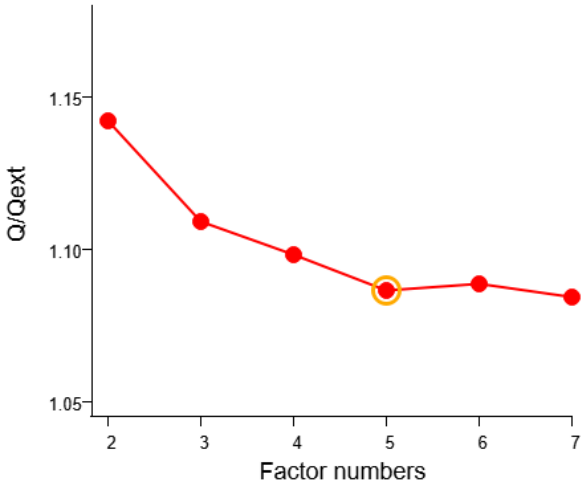

Figure S1. Q/Qexp as a function of the number of factors in PMF analysis

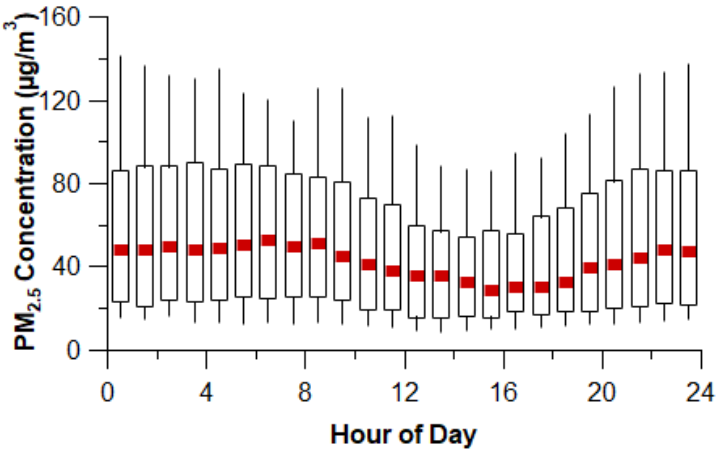

Figure S2. Diurnal variation of $PM_{2.5}$ concentration during the whole sampling period

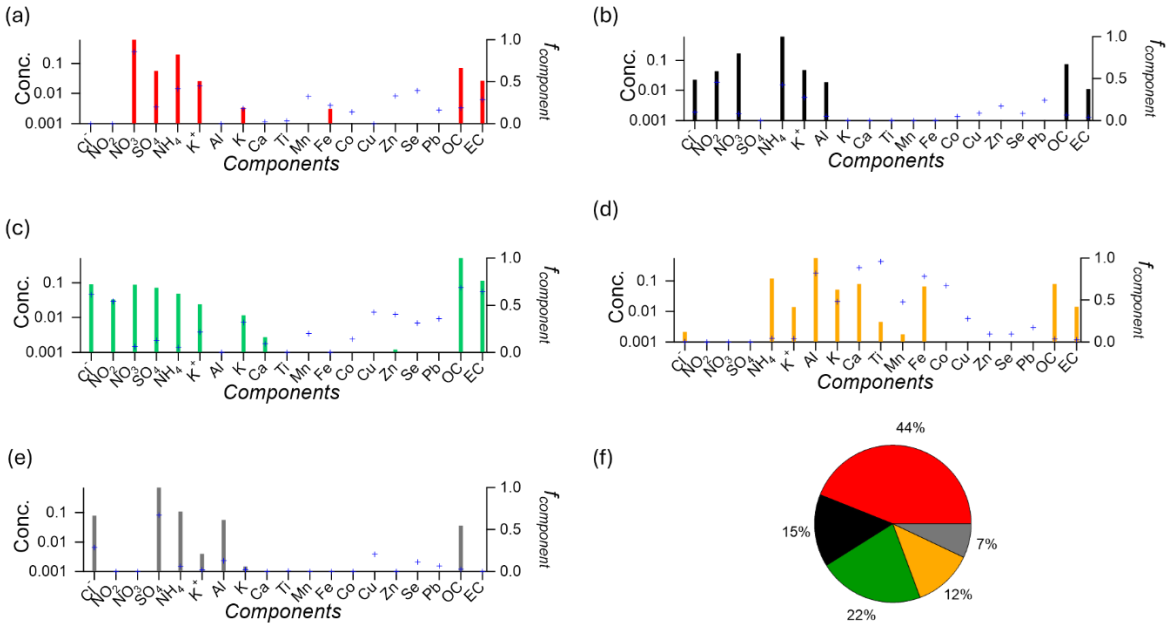

Figure S3. Resolved source profiles of $PM_{2.5}$ factors obtained from PMF analysis of online components: (a) secondary inorganics, (b) vehicle emissions, (c) biomass burning, (d) coal combustion, (e) dust emission, and (f) source contribution fraction of each source.

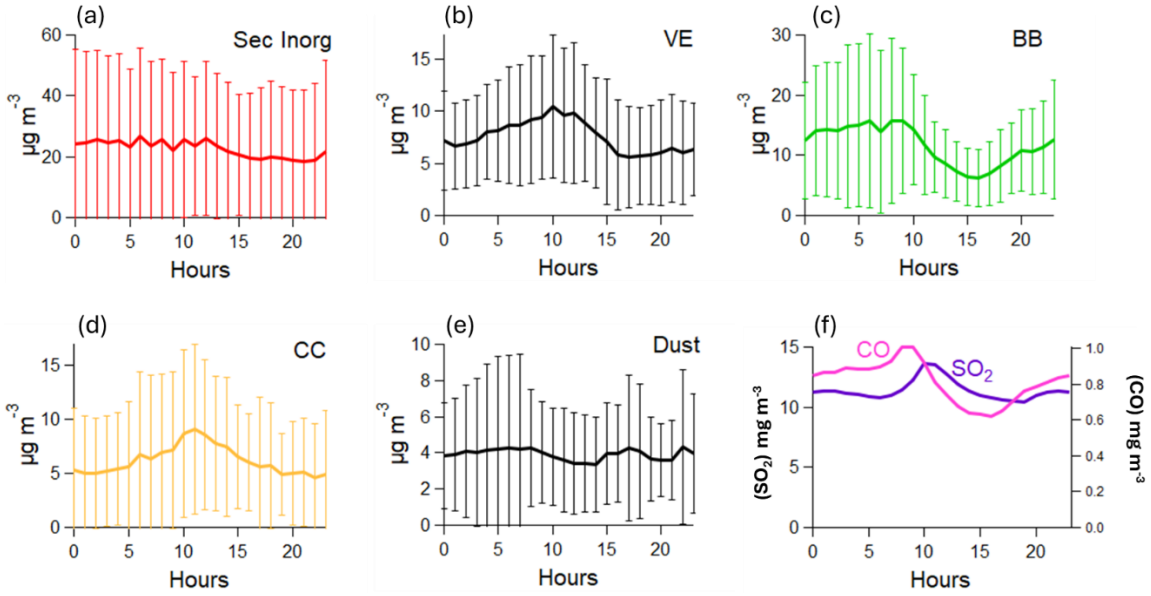

Figure S4. Diurnal variation of resolved sources and gaseous pollutants: (a) secondary inorganics, (b) vehicle emissions, (c) biomass burning, (d) coal combustion, (e) dust emission, and (f) CO and SO_2.

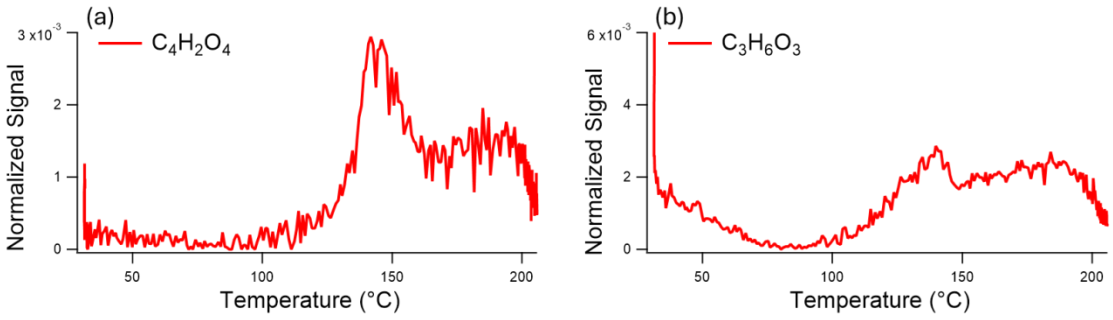

Figure S5. Thermogram for $C_4H_2O_4$ and $C_3H_6O_3$, the normalized signals versus desorption temperature were from January 6, 2024.

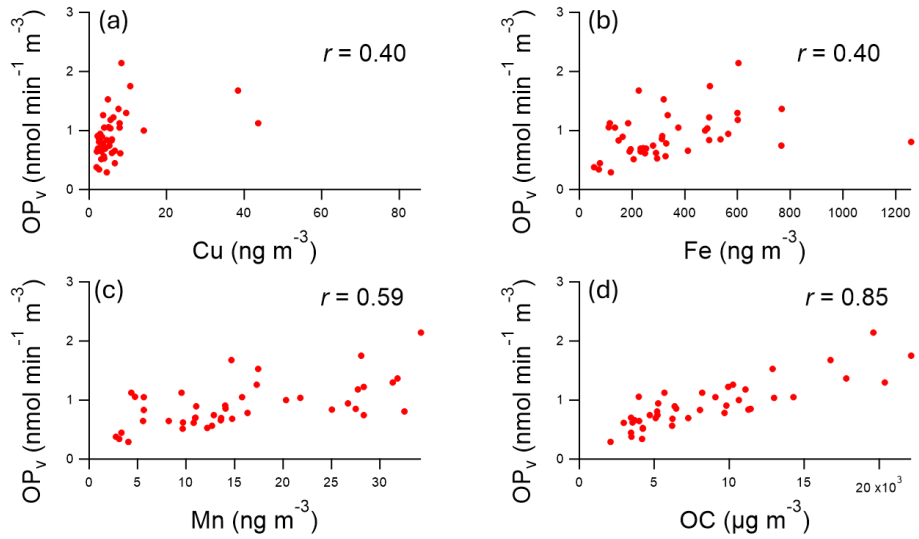

Figure S6. Correlation between OP_v (DTT) versus Cu, Fe, Mn and OC during our sampling period.

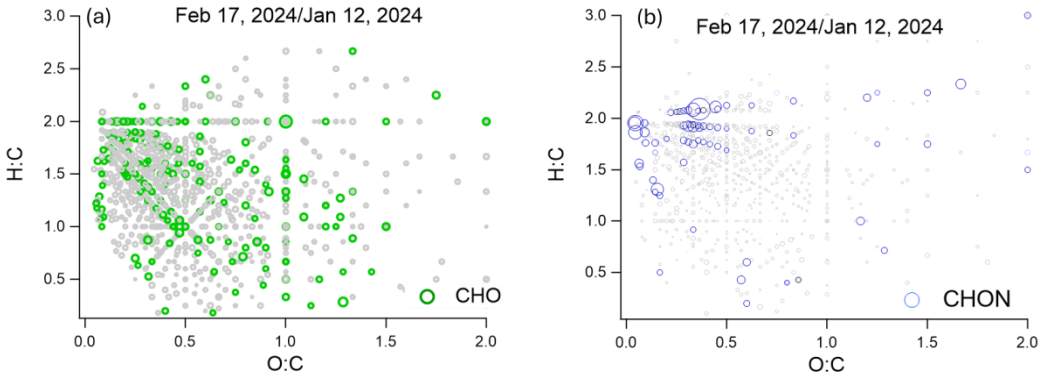

Figure S7. Van Krevelen (VK) diagrams for CHO and CHON compounds. Dot sizes are proportional to the square root of the signal ratios (February 17 vs. January 12) for the corresponding compounds. Grey dots indicate a signal ratio less than 1, while green (CHO) and blue (CHON) dots indicate a signal ratio greater than 1.

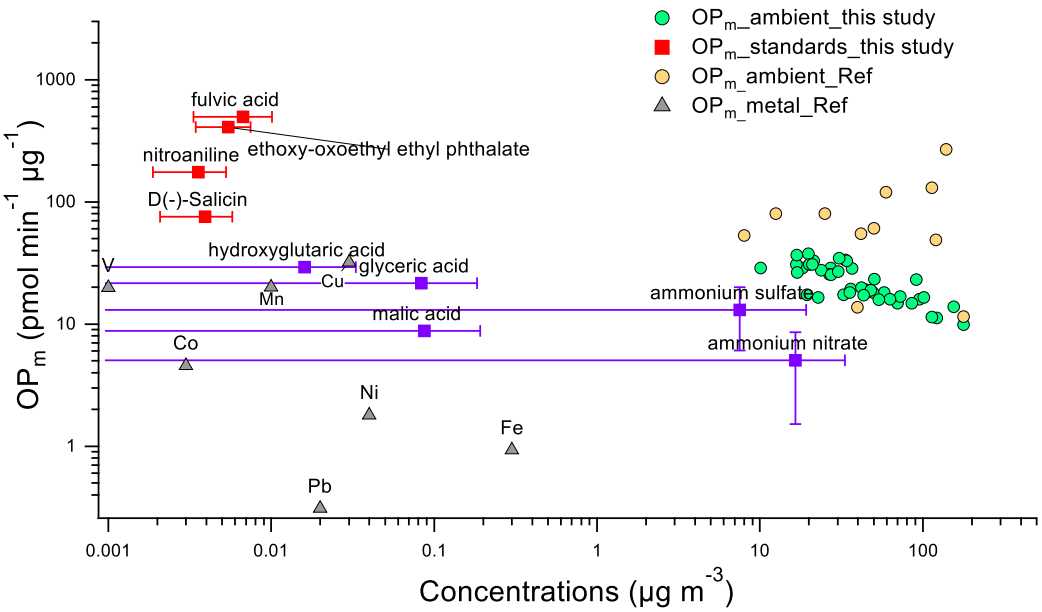

Figure S8. The OP_m of ambient samples and chemical standards under ambient atmospheric concentrations. Ambient samples are represented by circles, while chemical standards are shown as squares. Specifically, green circles denote ambient samples from our study, and yellow circles indicate values from previous literature. Red squares represent standard compounds that were positively correlated with OP_m, whereas purple squares represent those with a negative correlation. Grey triangles represent the OP_m from transit metals[5]. OP_m data determined in other sites is adapted from previous studies conducted in Athens[6], Beijing[7, 8], Los Angeles[9], Nanjing[10], NCP (rural)[11], New Delhi [12, 13], Paris[6], Tianjin[14], and Xi'an[15].

References

1. Koss, A. R.; Canagaratna, M. R.; Zaytsev, A.; Krechmer, J. E.; Breitenlechner, M.; Nihill, K. J.; Lim, C. Y.; Rowe, J. C.; Roscioli, J. R.; Keutsch, F. N.; Kroll, J. H., Dimensionality-reduction techniques for complex mass spectrometric datasets: application to laboratory atmospheric organic oxidation experiments. *Atmospheric Chemistry and Physics* **2020,** *20*, (2), 1021-1041.
2. Priestley, M.; Bannan, T. J.; Le Breton, M.; Worrall, S. D.; Kang, S.; Pullinen, I.; Schmitt, S.; Tillmann, R.; Kleist, E.; Zhao, D.; Wildt, J.; Garmash, O.; Mehra, A.; Bacak, A.; Shallcross, D. E.; Kiendler-Scharr, A.; Hallquist, Å. M.; Ehn, M.; Coe, H.; Percival, C. J.; Hallquist, M.; Mentel, T. F.; McFiggans, G., Chemical characterisation of benzene oxidation products under high- and low-NOx conditions using chemical ionisation mass spectrometry. *Atmospheric Chemistry and Physics* **2021,** *21*, (5), 3473-3490.
3. Wang, X. K.; Hayeck, N.; Bruggemann, M.; Yao, L.; Chen, H. F.; Zhang, C.; Emmelin, C.; Chen, J. M.; George, C.; Wang, L., Chemical Characteristics of Organic Aerosols in Shanghai: A Study by Ultrahigh-Performance Liquid Chromatography Coupled With Orbitrap Mass Spectrometry. *Journal of Geophysical Research-Atmospheres* **2017,** *122*, (21), 11703-11722.
4. Kroll, J. H.; Donahue, N. M.; Jimenez, J. L.; Kessler, S. H.; Canagaratna, M. R.; Wilson, K. R.; Altieri, K. E.; Mazzoleni, L. R.; Wozniak, A. S.; Bluhm, H.; Mysak, E. R.; Smith, J. D.; Kolb, C. E.; Worsnop, D. R., Carbon oxidation state as a metric for describing the chemistry of atmospheric organic aerosol. *Nature Chemistry* **2011,** *3*, (2), 133-139.
5. Charrier, J. G.; Anastasio, C., On dithiothreitol (DTT) as a measure of oxidative potential for ambient particles: evidence for the importance of soluble transition metals. *Atmospheric Chemistry and Physics* **2012,** *12*, (19), 9321-9333.
6. Tassel, C.; Jaffrezo, J.-L.; Dominutti, P.; Daellenbach, K. R.; Darfeuil, S.; Elazzouzi, R.; Laj, P.; Marsal, A.; Mhadhbi, T.; Dinh, V. N. T.; Voiron, C.; Houdier, S.; Durif, M.; Chatain, M.; Francony, F.; Cozic, J.; Salque Moreton, G.; Le Quilleuc, M.; Ghersi, V.; Gille, G.; Mesbah, B.; Stratigou, E.; Zublena, M.; Diémoz, H.; Alastuey, A.; D'Anna, B.; Marchand, N.; Conil, S.; Gros, V.; van Os, M. F.; Salma, I.; Mihalopoulos, N.; Močnik, G.; Džepina, K.; Styszko, K.; Hüglin, C.; Querol, X.; Prévôt, A. S. H.; Favez, O.; Siroux, V.; Uzu, G., Oxidative potential of atmospheric particles in Europe and exposure scenarios. *Nature* **2025,** *647*, (8088), 109-114.
7. Li, J.; Hua, C.; Ma, L.; Chen, K.; Zheng, F.; Chen, Q.; Bao, X.; Sun, J.; Xie, R.; Bianchi, F.; Kerminen, V.-M.; Petäjä, T.; Kulmala, M.; Liu, Y., Key drivers of the oxidative potential of PM2.5 in Beijing in the context of air quality improvement from 2018 to 2022. *Environment International* **2024,** *187*.
8. Yu, S.; Liu, W.; Xu, Y.; Yi, K.; Zhou, M.; Tao, S.; Liu, W., Characteristics and oxidative potential of atmospheric PM2.5 in Beijing: Source apportionment and seasonal variation. *Science of The Total Environment* **2019,** *650*, 277-287.
9. Shen, J.; Taghvaee, S.; La, C.; Oroumiyeh, F.; Liu, J.; Jerrett, M.; Weichenthal, S.; Del Rosario, I.; Shafer, M. M.; Ritz, B.; Zhu, Y.; Paulson, S. E., Aerosol Oxidative Potential in the Greater Los Angeles Area: Source Apportionment and Associations with Socioeconomic Position. *Environmental Science & Technology* **2022,** *56*, (24), 17795-17804.
10. Yang, F.; Liu, C.; Qian, H., Comparison of indoor and outdoor oxidative potential of PM2.5: pollution levels, temporal patterns, and key constituents. *Environment International* **2021,** *155*.
11. Cao, F.; Chen, Y.; Han, Y.; Chen, T.; Feng, X.; Jiang, H.; Zhang, Q.; Ma, H.; Li, J.; Zhang, G., Key toxicity enhancement effect of aqueous-phase secondary formation: Insights from hourly measurements during haze events. *Journal of Hazardous Materials* **2025,** *492*.
12. Verma, P. K.; Devaprasad, M.; Dave, J.; Meena, R.; Bhowmik, H.; Tripathi, S. N.; Rastogi, N., Summertime oxidative potential of atmospheric PM2.5 over New Delhi: Effect of aerosol ageing. *Science of The Total Environment* **2024,** *920*.
13. Pipal, A. S.; Ghude, S. D.; Satsangi, P. G.; Bhatkar, M. Y.; Kale, A.; Nivdange, S. S.; Rao, M. N.; Mukherjee, A.; Vispute, A. S.; Sharma, H.; Kumar, V.; Lonkar, P.; Kori, P.; Gosavi, S., Impact of primary

aerosol particles on size specific oxidative potential and its relationship with air quality and hazard index. *Atmospheric Environment* **2025,** *361*.
14. Liu, W.; Xu, Y.; Liu, W.; Liu, Q.; Yu, S.; Liu, Y.; Wang, X.; Tao, S., Oxidative potential of ambient PM2.5 in the coastal cities of the Bohai Sea, northern China: Seasonal variation and source apportionment. *Environmental Pollution* **2018,** *236*, 514-528.
15. Chen, Q. C.; Wang, M. M.; Wang, Y. Q.; Zhang, L. X.; Li, Y. G.; Han, Y. M., Oxidative Potential of Water-Soluble Matter Associated with Chromophoric Substances in PM2.5 over Xi'an, China. *ENVIRONMENTAL SCIENCE & TECHNOLOGY* **2019,** *53*, (15), 8574-8584.